

# Molecular Motor Propelled Filaments Reveal Light-Guiding in Nanowire Arrays for Enhanced Biosensing

Lasse ten Siethoff,<sup>†,||</sup> Mercy Lard,<sup>‡,||</sup> Johanna Generosi,<sup>‡,§</sup> Håkan S. Andersson,<sup>†</sup> Heiner Linke,<sup>‡</sup> and Alf Månsson<sup>\*,†</sup>

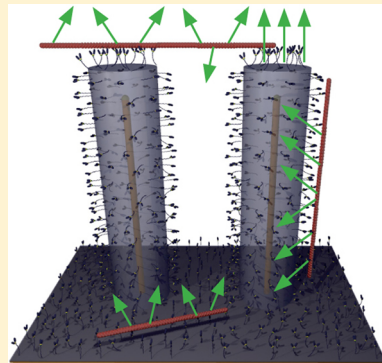
<sup>†</sup>Department of Chemistry and Biomedical Sciences, Linnaeus University, SE-391 82 Kalmar, Sweden

<sup>‡</sup>Nanometer Structure Consortium (nmC@LU) and Solid State Physics Lund University, SE-221 00 Lund, Sweden

## Supporting Information

**ABSTRACT:** Semiconductor nanowire arrays offer significant potential for biosensing applications with optical read-out due to their high surface area and due to the unique optical properties of one-dimensional materials. A challenge for optical read-out of analyte-binding to the nanowires is the need to efficiently collect and detect light from a three-dimensional volume. Here we show that light from fluorophores attached along several  $\mu\text{m}$  long vertical  $\text{Al}_2\text{O}_3$  coated gallium phosphide nanowires couples into the wires, is guided along them and emitted at the tip. This enables effective collection of light emitted by fluorescent analytes located at different focal planes along the nanowire. We unequivocally demonstrate the light-guiding effect using a novel method whereby the changes in emitted fluorescence intensity are observed when fluorescent cytoskeletal filaments are propelled by molecular motors along the wires. The findings are discussed in relation to nanobiosensor developments, other nanotechnological applications, and fundamental studies of motor function.

**KEYWORDS:** Nanobiotechnology, *in vitro* motility assay, photonics, actin, myosin, actomyosin



**A**rtificial semiconductor nanowires are elongated crystalline structures<sup>1</sup> with diameters and lengths in the 2–200 nm and 1–100  $\mu\text{m}$  ranges, respectively.<sup>2</sup> These nanostructures exhibit unique and designable optical properties, such as enhanced light absorption<sup>3</sup> and potential for optical wave-guiding<sup>2,4–6</sup> enabled by one-dimensional geometry, high refractive index (typically  $n > 2$ ) and the possibility of uniform diameter and coating with materials of different refractive index.

Because of their large surface-to-volume ratio, nanowires have attracted significant interest for biosensing both as scaffolds for recognition molecules such as antibodies or oligonucleotides and as a basis for specific signal transduction mechanisms utilizing their optoelectronic properties.<sup>7,8</sup> In particular, there are numerous reports (e.g., refs 9 and 10) of field-effect transistor (FET) based nanowire sensors with the nanowires generally located horizontally between electrodes. Biosensors based on vertical nanowire arrays with optical readout would offer much larger detection surface. Moreover, the possibility to use regular periodic arrays offers automated readout (see below) and ease of calibration. However, previous studies investigating the use of such nanowire arrays in biosensing for specific macromolecular detection are limited.<sup>5,7,11</sup> Particularly, to our knowledge, there are no prior reports of these types of studies focusing on the binding of fluorescent molecules to arrays of group III–V semiconductor (e.g., gallium phosphide, indium phosphide, and gallium arsenide) nanowires, which have advantageous optical properties.<sup>3,12,13</sup>

A major challenge in the use of nanowire arrays for fluorescence-based biosensors with optical readout is the limited depth of focus of high numerical-aperture objectives (suitable because of their high light-collection efficiency), preventing collection of emitted light from the array's entire volume. Furthermore, in biosensing it is generally challenging to provide clear evidence that a measured optical signal is indeed due to a specific interaction between sensor and analyte.

Here, we overcome both of these challenges. First, we report light guiding along oxide-coated gallium phosphide (GaP) nanowires with light collection from the entire nanowire length and focused emission from the tip, with appreciably increased signal-to-noise (S/N) ratio. This effect greatly enhances the potential of nanowire arrays for biosensing with optical readout. Second, we introduce a method that unambiguously demonstrates the light-guiding effect. Specifically, we use a unique approach where molecular motors propel several  $\mu\text{m}$  long fluorescent cytoskeletal filaments up and down the nanowires. As demonstrated below, this results in a verifiable and quantifiable time-variation of the number of probed fluorophores, an effect that may be practically useful in evaluation of nanobiosensor performance in general. The transportation of actin filaments in nanowire arrays also has implications for

**Received:** October 29, 2013

**Revised:** December 17, 2013

**Published:** December 24, 2013

development of three-dimensional lab-on-a-chip devices and fundamental studies of actomyosin function.

In the following, we first introduce oxide-coated GaP nanowire arrays as well as the actomyosin molecular motor system. We next show that myosin motor fragments are immobilized on the nanowires in a configuration that specifically binds actin filaments and propels them upon the addition of ATP. We then provide experimental evidence of light-guiding properties of the nanowires and their use to efficiently collect optical signals from fluorescent actin filaments, used as our test analyte. Finally, we discuss applications of our findings, particularly in biosensing.

**Actomyosin Motility Interfaced with Nanowire Arrays.** Muscle contraction is due to cyclic interactions between myosin II motor proteins and actin filaments powered by the cellular fuel adenosine-5'-triphosphate (ATP). In *in vitro* assays<sup>14,15</sup> one uses surface adsorbed myosin motors, or preferentially myosin motor fragments such as heavy meromyosin (HMM), to propel fluorescent actin filaments. Whereas such assays have inspired a range of nanotechnological applications,<sup>16–20</sup> actin and myosin have not previously been interfaced with vertical nanowire arrays.

We chose GaP as our material system because of the established biocompatibility of GaP nanowires<sup>21</sup> and the generally advantageous optical properties of the III–V semiconductor materials.<sup>3,12,13</sup> Nanowires were produced by gold-particle-seeded metal organic vapor phase epitaxy (MOVPE)<sup>22</sup> (Figures 1a and S1). Because nanowire growth is initialized by GaP assembly at the interface of the substrate to the gold particle, the wire size and array geometry (Figures 1a

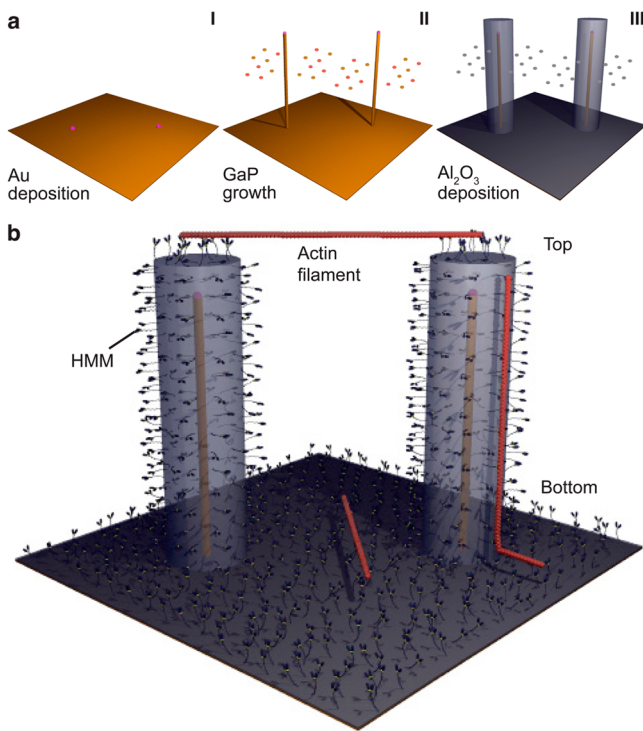


**Figure 1.** Principle of experiments. a, Nanowires are grown from gold seed particles (I) by metal organic vapor phase epitaxy (II) and coated with  $\text{Al}_2\text{O}_3$  by atomic layer deposition (III). b, Schematic illustration of fluorescently labeled actin filaments (red) that are propelled by HMM motors adsorbed to the  $\text{Al}_2\text{O}_3$  surface of nanowires. Note, illustration not to scale.

and 2a) can be defined by electron beam lithography (EBL)-defined gold patterning. The use of regular nanowire spacing

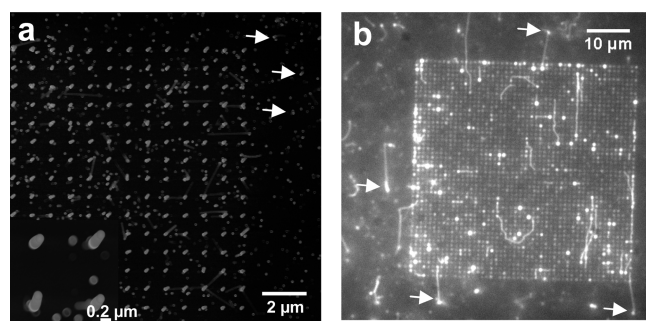


**Figure 2.** Nanowire arrays. a, Scanning electron microscopy (SEM) image of nanowires in  $50 \times 50 \mu\text{m}^2$  array with  $1 \mu\text{m}$  interwire distance and  $5 \mu\text{m}$  nanowire length. Close up view in inset. b, Fluorescence micrograph from *in vitro* motility assay experiment with the same type of array geometry as in panel a before the addition of ATP. Focus is kept on the top of the nanowires. Actin filaments (bright fluorescent lines) are aligned with nanowire arrays being attached to HMM on the tip of the nanowires. Strongly fluorescent spots on nanowires attributed to light-guiding from fluorescent actin filaments interacting with the wires along their length. Occasional fluorescent spots outside the array in panel b (arrows) are attributed to actin filaments attached to nanowires spuriously formed by parasitic growth (examples of such wires also indicated in panel a) and are therefore in focus.

enables the growth of arrays with uniform wire length. After testing several surface derivatization procedures (see Supporting Information, results section) with respect to actomyosin motility quality (speed and fraction of mobile actin filaments) we chose atomic layer deposition of  $\text{Al}_2\text{O}_3$  on nanowires (Figure 1a) and surrounding areas, creating suitable surface contact angles for motility<sup>23</sup> without the need for prior silanization. Together with the GaP nanowire core diameter ( $30\text{--}50 \text{ nm}$  in different arrays), the  $60 \text{ nm}$  of  $\text{Al}_2\text{O}_3$  coating resulted in a total nanowire diameter of  $150\text{--}171 \text{ nm}$  ( $\sim 160 \text{ nm}$  unless otherwise stated). The wire length was either  $0.96 \pm 0.03$  or  $5 \pm 0.2 \mu\text{m}$  (mean  $\pm$  standard deviation) in different arrays. *In vitro* motility studies were performed<sup>14</sup> by infusing HMM ( $120 \mu\text{g/mL}$ ) into flow cells formed by a chip with nanowire arrays (Figure 1) as the ceiling and a coverslip as the floor. Irrespective of the actual geometry, “top” and “bottom” in the text below are defined as indicated in Figure 1b. The HMM-induced sliding of Alexa Fluor 488 phalloidin labeled actin filaments was observed after infusion of assay solution ( $1 \text{ mM MgATP}$ ;  $22\text{--}25^\circ\text{C}$ ). The filaments were observed using epi-fluorescence microscopy. We used a Nikon Eclipse TE300 inverted microscope with Hg-lamp illumination, Nikon  $100 \times 1.4 \text{ NA}$  oil immersion objective, FITC filter set [excitation,  $465\text{--}495 \text{ nm}$ ; dichroic mirror cutoff,  $505 \text{ nm}$ ; emission barrier filter,  $515\text{--}555 \text{ nm}$ ] and a Hamamatsu EMCCD camera. Further details of the experimental methods are given in the Supporting Information, methods section, e.g., quantitative analysis of the motility quality of filaments moving up and down wires (Supporting Figures S2–S3).

We found that actin filaments can be bound to and propelled by HMM adsorbed to  $\text{Al}_2\text{O}_3$ -coated GaP nanowires. First, we infused fluorescent actin filaments in the absence of ATP where HMM is expected to bind the filaments but not propel them. Under these conditions, filaments attached themselves horizontally across the top (Figure 1b) of a nanowire array,

apparently binding to multiple nanowire tips (Figure 2). In addition, several strongly fluorescent spots were associated with individual wires in sparse (interwire distance 1  $\mu\text{m}$ ; Figure 2) arrays and along the edges in denser arrays (interwire distance < 300 nm; not shown). We attribute these spots to filaments that are attached vertically along individual wires (see below). Upon addition of ATP, we observed actin motility on areas surrounding the nanowire arrays (Figure 3a) as well as on top

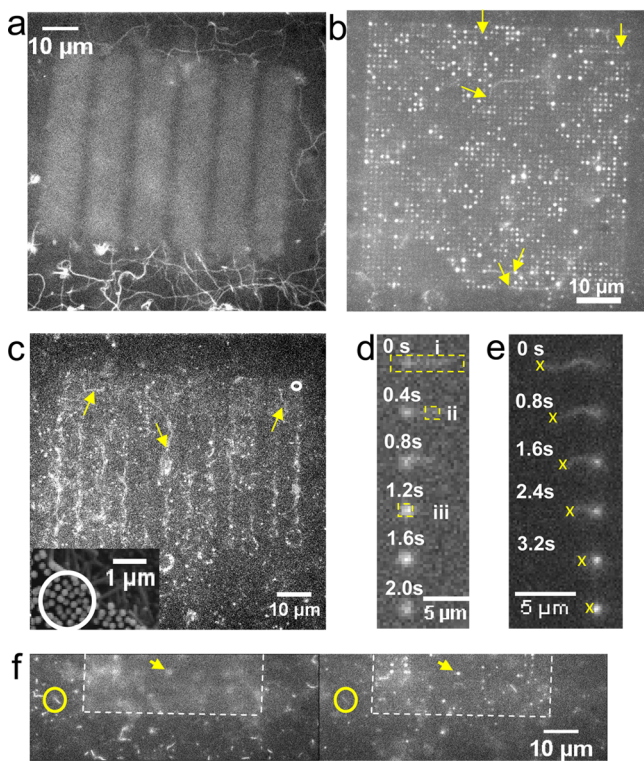


**Figure 3.** Actomyosin motility on nanowire arrays analyzed by fluorescence microscopy. a, Motility on  $\text{Al}_2\text{O}_3$  surface outside autofluorescent array illustrated by maximum pixel intensities over 50 consecutive images at  $2.5 \text{ s}^{-1}$  frame rate. Filament trajectories indicated as winding continuous lines. b, The maximum pixel intensity in sequence of 220 images at  $2.5 \text{ s}^{-1}$  frame rate for array with 1  $\mu\text{m}$  interwire distance and 5  $\mu\text{m}$  nanowire length. Arrows show starting points for some trajectories of actin filaments sliding on top of the array. c, Image sequence of array with circular and square nanowire patterns connected by zigzag lines with nanowires. Examples of filament trajectories indicated by arrows. Average interwire spacing: 250 nm (cf. scanning electron micrograph in inset showing area on another array similar to that in circle in main figure). d,e, Time sequence of filaments climbing down and up a nanowire, respectively. For dashed rectangles in panel d, see Figure 4c. The crosses in panel e indicate tracking of the trailing filament end to estimate the length of the filament segment that is vertically attached along the nanowire (fluorescent spot of increasing intensity) at each given point in time. f, Fluorescence images where focus changed from the bottom surface (left) to the top of the wires (right). See also Supporting Information Movie 3 and Figure S4 for similar effects of change in focus on another area.

of arrays having interwire distance of 1  $\mu\text{m}$  (Figure 3b; Supporting Information, Movie 1) and <300 nm (Figure 3c; Supporting Information, Movie 2). The filaments on the top moved from tip to tip, and, ultimately, some of them were propelled vertically down the wires (Figure 3d). Occasionally, filaments were also observed climbing up wires from the

surrounding surface (Figure 3e). However, observation of the latter phenomenon with 5  $\mu\text{m}$  long nanowires required refocusing of the microscope because the underlying substrate and the top of the nanowire array were located in different focal planes (Figure 3f). This fact was important as it also enabled us to unambiguously identify the plane in which filaments were moving (see also Supporting Information, Figure S4 and Movie 3).

A climbing event, whether up or down a wire, was associated with an initial rapid increase in intensity of a fluorescent spot centered on the wire (Figure 3; Supporting Information, Movie 1), followed by rapid decline in fluorescence of this spot (see further below). Such intensity variations (“blinking”) were not observed in the absence of ATP, and they were seen in all cases where the filament transition from horizontal to vertical movement could be directly observed. Therefore, we attribute observed blinking events to motile actin filaments.

**Light-Guiding by Nanowires.** By observing individual actin filaments first approach and then climb up or down individual nanowires, we could identify and quantify light guiding of fluorescent emission from actin filaments specifically bound to nanowires. On a sparse array (nanowire length 5  $\mu\text{m}$ , interwire distance 1  $\mu\text{m}$ ), filaments that climbed up or down wires were visible from the top as strongly fluorescent spots (Figure 3b; also Figure 2b, Figure S2 and Supporting Information, Movie 1) with a time-dependent intensity proportional to the fraction of the filament length attached vertically along the wire via HMM. Importantly the number of fluorophores along the wires, at each given point in time, is directly proportional to the filament length along the wire in a well characterized way. This follows because there is precisely one binding site for the APH fluorophore per actin monomer.<sup>24,25</sup> Further, the distance between the monomers is well-known<sup>26</sup> giving 362 APH binding sites per  $\mu\text{m}$  (see further Supporting Information, methods). Thus, taking advantage of this homogeneous fluorescence labeling, we were able to estimate, with good accuracy, the number of fluorophores on the filament segments along the wire by tracking the trailing end of individual filaments whose leading end progressed up or down the wire (Figure 3e). Results of such tracking for three filaments climbing 5  $\mu\text{m}$  long nanowires are illustrated in Figure 4a, together with intensity measurements that show progressive linear increase in intensity ( $I_{\text{tip}}$ ) emitted from the nanowire tip as the filament length along the wire increases. Further, this intensity saturated at low values (Figure 4b) for nanowires with length of less than 1  $\mu\text{m}$  (Supporting Information, Figure S5), whereas the maximum intensity  $I_{\text{tip}}$  for filaments moving along 5  $\mu\text{m}$  long nanowires increased in proportion to the maximum intensity ( $I_h$ ; proportional to length) measured when the filaments moved horizontally. The results for the two wire lengths show that only the part of the filament held close to the wire surface contributes significantly to the fluorescence signal. More importantly, however, the results in Figure 4a,b for 5  $\mu\text{m}$  long wires cannot be explained by, for example, the projection of fluorescence of vertically aligned filaments because the depth of focus of our objective (<0.6  $\mu\text{m}$ ; Figure 3f; Supporting Information, Figure S4 and Movie 3), was much too limited to collect light from all along the nanowire. Instead, light-collection and light-guiding by the nanowire is necessary to integrate the filament fluorescence intensity into a nearly diffraction limited spot, in the focal plane of the wire tip. This view is further supported by the effects of changes in focus on

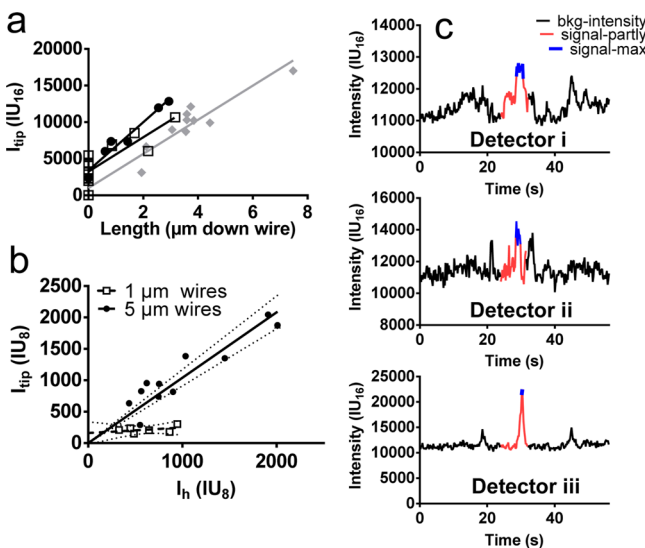


**Figure 4.** Signal intensity analysis of nanowire light-guiding on sparse arrays. **a**, Average background-subtracted pixel fluorescence intensity from the tip of nanowires ( $0.5 \times 0.5 \mu\text{m}^2$  region of interest (ROI); 16 bit images; intensity units,  $\text{IU}_{16}$ ) plotted against the distance that three different filaments (different symbols) have moved down a wire of  $5 \mu\text{m}$  length. The nonzero intercept on the vertical axis is due to the tip of horizontally moving filaments entering the ROI without movement of the trailing filament end that is tracked. This may occur for filaments moving on top of a sparse nanowire array as the number of strongly attached actin propelling heads on the wire tips vary with time. Thus, the leading filament end would temporarily move faster than the tracked trailing end due to buckling caused by previous faster sliding of the trailing end. Measurements using ImageJ. **b**, Total background-subtracted fluorescence intensity ( $I_{\text{tip}}$ ; average intensity  $\times$  number of pixels) observed from nanowire tip due to nanowire-climbing filaments plotted against the total intensity ( $I_h$ ) of the same filaments when sliding on top of the array (for  $5 \mu\text{m}$  high nanowires; filled circles) or on the surface between nanowires ( $0.96 \mu\text{m}$  wires; open squares). Measurements using Matlab after conversion to 8 bit images corresponding to units,  $\text{IU}_8$ . **c**, Time course of the fluorescence signal at three different locations as indicated in Figure 3d, illustrating the potential to use the light guiding effect for fluorescence detection with increased signal/noise ratio. Measurement using ImageJ and 16 bit images showing average intensity per pixel. For details of ImageJ and Matlab-based analyses, see Supporting Information (methods).

the intensity (Supporting Information, Figure S4) measured within a  $0.5 \times 0.5 \mu\text{m}^2$  ROI centered on a nanowire.

Interestingly, the behavior was different in denser nanowire arrays ( $<300 \text{ nm}$  spacing) where similar apparent light-guide effects were mainly observed at edges (indicated by strong fluorescent spots in Figure 3c; see also Supporting Information, Movie 2).

Quantitatively, we estimate that  $\sim 50\%$  of the light emitted from fluorescent actin filaments attached vertically along wires in sparse ( $1 \mu\text{m}$  interwire distance) arrays is emitted from their tip. We draw this conclusion, first, from the measured slope near unity ( $\sim 1.04$ ; 95% CI [0.91, 1.17]) of the observed linear relationship ( $r \approx 0.91$ ) between  $I_{\text{tip}}$  and  $I_h$  for nanowires of  $5 \mu\text{m}$  length (Figure 4b). Second, we reasonably assume that less than 50% of the light from a filament (moving in an optically homogeneous environment across the nanowire tips) is available for collection by the objective. We further note that our experimental setup does not fulfill any geometrical conditions for intensity enhancement (neither of  $I_{\text{tip}}$  nor  $I_h$ ) by fluorescence interference contrast effects.<sup>27</sup> Our results are

thus consistent with the notion that the entire emitted fluorescence intensity from a fluorescence labeled actin filament, held by HMM along a nanowire in a sparse array, couples into the wire and that 50% of the light intensity is emitted at the wire tip, whereas 50% enters the surface substrate. In this context it is important to note that zincblende GaP has a direct band gap of  $2.78 \text{ eV}$ , corresponding to  $450 \text{ nm}$  light wavelength. This should be compared to excitation wavelengths in the range  $465\text{--}495 \text{ nm}$  and emission in the range  $500\text{--}600 \text{ nm}$  (observed in range  $515\text{--}555 \text{ nm}$  with the current microscope filter set). Therefore, the GaP nanowires and the underlying GaP substrate should absorb and reflect light only to a minor degree.

Our observations of efficient coupling of light into the GaP nanowires and light guiding along these wires are consistent with previous findings using other semiconductor materials.<sup>2,4\text{--}6,28</sup> In those prior studies, photonic confinement was shown for a range of nanowires (e.g., ZnO, CdS, GaN, and GaSb) acting as single lasers under optical pumping.<sup>2,5</sup> Their high refractive index and the surrounding dielectric material allow for wave-guiding with amplified output. Furthermore, enhanced light trapping and emission has been observed using light coupled into tips of III-V semiconductor nanowires that are grown in ordered arrays and coated with a dielectric material with a smaller refractive index than the core (e.g.,  $\text{Al}_2\text{O}_3$ ).<sup>13</sup> The degree of enhancement appeared to depend on fine-tuning of the dimensions of the III-V core, the  $\text{Al}_2\text{O}_3$  layer, and the array spacing. This is consistent with our observations of different degrees of light guiding for different interwire distances and suggests that there is appreciable room for optimization of light collection and emission in future experiments.

**Applications of Light-Guiding.** Our demonstration of light-guiding of GaP nanowires in a biological buffer has a range of interesting applications in biosensing (see also ref 5). Thus, the nanowires would perform well as optical sensors that capture analyte molecules via recognition elements (e.g., antibodies or oligonucleotides) immobilized on their large surface areas. If fluorescent secondary recognition molecules are sandwiched via the analytes to the nanowires, light intensity proportional to the number of such recognition molecules would be emitted from the wire tip. In the following, we illustrate and quantify the advantages of this approach using a specific example where the velocity and fraction of motile actin filaments are evaluated. High-throughput assays with this capability are of considerable interest per se, e.g., to evaluate effects of drugs<sup>29,30</sup> on actomyosin motility. The efficient detection of actin filaments<sup>31</sup> is also important in motor-driven diagnostics<sup>18,32</sup> and biocomputation devices.<sup>17</sup>

The achievable S/N ratio for the detection of actin filament speed using nanowire arrays is much higher than that achievable on flat substrates and automated read-out is greatly simplified (see below). We quantify the fraction of motile filaments by the ratio of the numbers of time-varying and time-invariant fluorescent spots (Figure S2, Supporting Information) and determine the filament velocity from the rate of change of the fluorescence intensity (Figure 4a; see also Figure S3, Supporting Information). The fraction of motile filaments and velocity for nanowire-climbing actin filaments determined in this way was  $81 \pm 3.8\%$  (mean  $\pm$  standard error of the mean; SE;  $n = 136$  filaments) and  $2.18 \pm 0.38 \mu\text{m/s}$  ( $n = 10$  filaments), respectively, compared to  $84 \pm 3.9\%$  ( $n = 83$ ) and  $5.16 \pm 0.15 \mu\text{m/s}$  ( $n = 22$ ), respectively, for a standard

trimethylchlorosilane (TMCS)-derivatized<sup>33</sup> flat surface. Crucially, however, the time-varying fluorescence intensity for a filament moving down a nanowire was detected with considerably higher S/N ratio than for a horizontally moving filament (Figure 4c). To exemplify, for two different filaments the S/N ratio was 13 and 17, respectively, when moving down a wire (using a region of interest [ROI] of  $0.5 \times 0.5 \mu\text{m}^2$ ; Figure 4c) compared to less than 4 when the filaments moved on top of the nanowire array (whether using small,  $0.5 \times 0.5 \mu\text{m}^2$  or large rectangular ROIs; Figure 3d). Qualitatively similar data were observed for several more filaments and also for filaments that first moved on the flat underlying substrate and then climbed up wires.

Under the present, far from optimized conditions (see below), the limit of detection (LOD) was 50–100 fluorophores on individual wires as suggested by observation of the photobleaching of stationary actin filaments attached via HMM to the wires, assuming 362 fluorophores per  $\mu\text{m}$  of an actin filament (see above and Supporting Information, methods). Here, the LOD was defined as the number of fluorophores that could be detected with S/N ratio of 3 or greater. The number of 50–100 fluorophores per wire corresponds to the amount of protein accumulating on the surface of a nanowire with  $\sim 100 \text{ nm}$  diameter in less than 1 h at 1 pM solution concentration.<sup>34</sup> However, importantly the LOD is probably somewhat lower than 50–100 fluorophores as there is most likely less than 362 monomers per  $\mu\text{m}$  of the filament, e.g., due to prior photobleaching events.

Averaging the signal over a large number of wires ( $n_{\text{wire}}$ ) would increase the S/N ratio in proportion to  $(n_{\text{wire}})^{1/2}$ . For instance, a 100-fold increase in S/N ratio would be achieved by averaging over 10 000 nanowires, which could be readily fitted into  $<100 \times 100 \mu\text{m}^2$  area. This would allow detection of analyte at 1 pM concentration in minutes or 10 fM concentration in an hour.<sup>34</sup> Unlike in the present study where actin filaments were bound to only a small fraction of the nanowires, recognition elements and analytes in biosensor applications are expected to bind to all nanowires in regular arrays with equal probability. The averaging should therefore be readily automated, e.g., by appropriately adjusting array interwire distance, objective magnification, and CCD pixel size to each other.

Several additional improvements would markedly increase the S/N ratio and further lower the LOD. This includes oblique illumination of the observation area together with reduced flow-cell height for reduced out-of-focus background and use of laser illumination instead of an Hg lamp to increase excitation intensity at 480 nm wavelength. Furthermore, a major source of noise, absent in a general biosensor application, is attributed to fluorescent actin filaments floating in solution. These unbound model analytes were not eliminated by rinsing as would be implemented for any other analyte, following specific binding to recognition molecules on the wires. Finally, it is likely that a theoretical analysis of the underlying optical mechanisms would allow optimization of the in- and out-coupling of light, further enhancing S/N ratio. Thus, the fluorescence wavelength, the nanowire material, length, diameter, spacing, and the thickness of the oxide shell might affect coupling of light into the wire. This coupling may also depend on the distance of the fluorophore to the nanowire surface (40 nm for HMM–actin),<sup>35</sup> the position of the emitting fluorophores along the wire,<sup>6</sup> and the polarization of fluorescence.

## New Method for Evaluating Biosensor Performance.

A second key result of our study is the unique method to unambiguously demonstrate specific analyte–detector interaction using molecular motor propelled cytoskeletal filaments. This was enabled by (i) measurement of the length of overlap between a fluorescence labeled filament and the long axis of the nanowire, (ii) a well-defined number of fluorophores per  $\mu\text{m}$  of the filament, and (iii) molecular-motor driven variation of the filament–nanowire overlap. Here we used heavy meromyosin propelled actin filaments labeled with a maximum of one fluorophore per monomer ( $\leq 362 \text{ monomers}/\mu\text{m}$ )<sup>26</sup> via the strong phalloidin–actin interaction. However, other motor systems, such as the kinesin-microtubule system, may also be used, enabling wide applicability due to different dependence of motor function on surface chemistry (cf. ref 36) for the two systems. Furthermore, other detectors should be possible to study by similar approaches.

**Further Implications of Results.** To the best of our knowledge, the present results also constitute the first demonstration of actomyosin motility on  $\text{Al}_2\text{O}_3$  substrate and on vertical nanowire arrays, opening for a range of opportunities. First, the observed climbing of filaments along nanowires enables three-dimensional motor driven lab-on-a-chip devices. Second, the observation of actin filament propulsion across the tips of 160 nm wide nanowires at 1  $\mu\text{m}$  interwire spacing opens for unique studies of actomyosin function. For instance, it will allow testing of hypotheses about the motility of actin filaments over a sparse layer of motors<sup>37</sup> with minimal interference from surface–actin interactions when filaments move from tip to tip. Such studies are relevant for understanding fundamental cooperative phenomena. They are also of interest for studying contractile events at low myosin densities on actin filaments as occurs physiologically at low activation levels in muscle cells when only a fraction of the regulatory units along the filament are turned on to allow myosin binding. For developments of functional assays it may be beneficial to make the vertical parts of the nanowires resistant to HMM binding in analogy to a previous study where kinesin propelled microtubules were observed moving between tips of micrometer wide poly(dimethylsiloxane) (PDMS) pillars.<sup>38</sup>

**Conclusions.** We have demonstrated light guiding with high efficiency along  $\text{Al}_2\text{O}_3$  coated GaP nanowires of appreciable relevance for biosensing applications. With further improved S/N ratio as discussed, sensor elements based on individual vertical nanowires could achieve fM–pM sensitivity, and arrays of such nanowires could perform appreciably better. The use of molecular motor driven propulsion of fluorescent filaments along the nanowires to detect specific molecular interactions may have broad applicability in the evaluation of biosensor performance. In addition, our findings lay the foundations for novel types of fundamental studies and nanotechnological applications of molecular motors.<sup>18,32</sup>

## ■ ASSOCIATED CONTENT

### ■ Supporting Information

Detailed description of the experimental procedures and data analysis (Methods); results from experiments leading up to the use of  $\text{Al}_2\text{O}_3$  as surface substrate for actomyosin motility; results from motility on surfaces with nanowire arrays with short (0.96  $\mu\text{m}$ ) nanowires; and quantitative analysis of the effect of altered plane of focus on observed fluorescence intensity. Furthermore, three movies are included. Two of these illustrate

HMM propelled sliding of actin filaments on sparse ( $1\ \mu\text{m}$  interwire distance) and dense ( $<300\ \text{nm}$  interwire distance) nanowire arrays, respectively. The third movie illustrates the effect of changing the plane of focus from the top to the bottom of the nanowire array. This material is available free of charge via the Internet at <http://pubs.acs.org>.

## AUTHOR INFORMATION

### Corresponding Author

<sup>\*</sup>(A.M.) E-mail: alf.mansson@lnu.se.

### Present Address

<sup>§</sup>(J.G.) Nano-Science Center, Department of Chemistry, University of Copenhagen, DK-2100 Copenhagen, Denmark.

### Author Contributions

<sup>¶</sup>L.t.S. and M.L. contributed equally to this work. A.M. and H.L. designed the study and supervised research, L.t.S. and M.L. performed *in vitro* motility assay studies, L.t.S. and H.A. developed surface functionalization procedures, M.L. and J.G. performed nanofabrication, and A.M., L.t.S., M.L., and J.G. analyzed data. All authors collaborated on writing the paper.

### Notes

The authors declare the following competing financial interest(s): A.M. is a co-founder, co-owner, and CEO of the start-up company ActoSense Biotech AB (Kalmar, Sweden) aiming to develop diagnostic devices based on the aggregation of cytoskeletal elements, particularly actin filaments, in solution. Moreover, A.M. holds two Swedish patents and one US patent in this field, and application for one of these patents has also been filed in Europe. Finally, A.M. and L.t.S. have submitted one additional Swedish patent application with molecular motors and actin filaments in focus.

## ACKNOWLEDGMENTS

We thank Nicklas Anttu for valuable discussions on the interaction of light and nanowire arrays. This work was funded by the European Union Seventh Framework Programme (FP7/2007-2011) under grant agreement number 228971 (MONAD), the Swedish Research Council (Projects # 621-2010-5146 and 621-2010-4527), the Carl Trygger Foundation, the Crafoord Foundation, the Faculty of Natural Sciences and Engineering and the Faculty of Health and Life Sciences at Linnaeus University, the Nanometer Structure Consortium (nmC@LU), and the Knut and Alice Wallenberg Foundation.

## REFERENCES

- (1) Dick, K. A. *Prog. Cryst. Growth Charact.* **2008**, *54*, 138–173.
- (2) Yan, R. X.; Gargas, D.; Yang, P. D. *Nat. Photonics* **2009**, *3*, 569–576.
- (3) Wallentin, J.; Anttu, N.; Asoli, D.; Huffman, M.; Aberg, I.; Magnusson, M. H.; Siefer, G.; Fuss-Kailuweit, P.; Dimroth, F.; Witzigmann, B.; Xu, H. Q.; Samuelson, L.; Deppert, K.; Borgstrom, M. T. *Science* **2013**, *339*, 1057–1060.
- (4) Law, M.; Sirbuly, D. J.; Johnson, J. C.; Goldberger, J.; Saykally, R. J.; Yang, P. *Science* **2004**, *305*, 1269–1273.
- (5) Sirbuly, D. J.; Law, M.; Pauzauskis, P.; Yan, H. Q.; Maslov, A. V.; Knutsen, K.; Ning, C. Z.; Saykally, R. J.; Yang, P. D. *Proc. Natl. Acad. Sci. U.S.A.* **2005**, *102*, 7800–7805.
- (6) Paniagua-Dominguez, R.; Grzela, G.; Rivas, J. G.; Sanchez-Gil, J. A. *Nanoscale* **2013**, *5*, 10582–10590.
- (7) Kar, P.; Shankar, K. *J. Nanosci. Nanotechnol.* **2013**, *13*, 4473–4496.
- (8) Curreli, M.; Zhang, R.; Ishikawa, F. N.; Chang, H. K.; Cote, R. J.; Zhou, C.; Thompson, M. E. *IEEE Trans. Nanotechnol.* **2008**, *7*, 651–667.
- (9) Cui, Y.; Wei, Q.; Park, H.; Lieber, C. M. *Science* **2001**, *293*, 1289–1292.
- (10) Zheng, G.; Patolsky, F.; Cui, Y.; Wang, W. U.; Lieber, C. M. *Nat. Biotechnol.* **2005**, *23*, 1294–1301.
- (11) Balasubramanian, K. *Biosens. Bioelectron.* **2010**, *26*, 1195–1204.
- (12) Chen, C. P.; Ganguly, A.; Wang, C. H.; Hsu, C. W.; Chattopadhyay, S.; Hsu, Y. K.; Chang, Y. C.; Chen, K. H.; Chen, L. C. *Anal. Chem.* **2009**, *81*, 36–42.
- (13) Anttu, N.; Namazi, K. L.; Wu, P. M.; Yang, P. F.; Xu, H. X.; Xu, H. Q.; Hakanson, U. *Nano Res.* **2012**, *5*, 863–874.
- (14) Kron, S. J.; Toyoshima, Y. Y.; Uyeda, T. Q.; Spudich, J. A. *Methods Enzymol.* **1991**, *196*, 399–416.
- (15) Kron, S. J.; Spudich, J. A. *Proc. Natl. Acad. Sci. U.S.A.* **1986**, *83*, 6272–6276.
- (16) Månnsson, A. *J. Muscle Res. Cell Motil.* **2012**, *33*, 219–233.
- (17) Nicolau, D. V.; Nicolau, D. V.; Solana, G.; Hanson, K. L.; Filipponi, L.; Wang, L. S.; Lee, A. P. *Microelectron. Eng.* **2006**, *83*, 1582–1588.
- (18) Korten, T.; Månnsson, A.; Diez, S. *Curr. Opin. Biotechnol.* **2010**, *21*, 477–488.
- (19) Agarwal, A.; Hess, H. *Prog. Polym. Sci.* **2010**, *35*, 252–277.
- (20) Byun, K. E.; Heo, K.; Shim, S.; Choi, H. J.; Hong, S. *Small* **2009**, *5*, 2659–2664.
- (21) Piret, G.; Perez, M. T.; Prinz, C. N. *Biomaterials* **2013**, *34*, 875–887.
- (22) Suyatin, D. B.; Hallström, W.; Samuelson, L.; Montelius, L.; Prinz, C. N.; Kanje, M. *J. Vac. Sci. Technol., B* **2009**, *27*, 3092–3094.
- (23) Albet-Torres, N.; O'Mahony, J.; Charlton, C.; Balaz, M.; Lisboa, P.; Aastrup, T.; Mansson, A.; Nicholls, I. A. *Langmuir* **2007**, *23*, 11147–11156.
- (24) Steinmetz, M. O.; Stoffler, D.; Muller, S. A.; Jahn, W.; Wolpensinger, B.; Goldie, K. N.; Engel, A.; Faulstich, H.; Aeby, U. *J. Mol. Biol.* **1998**, *276*, 1–6.
- (25) DelaCruz, E. M.; Pollard, T. D. *Biochemistry* **1996**, *35*, 14054–14061.
- (26) Hild, G.; Bugyi, B.; Nyitrai, M. *Cytoskeleton* **2010**, *67*, 609–629.
- (27) Lambacher, A.; Fromherz, P. *Appl. Phys. A: Mater. Sci. Process.* **1996**, *63*, 207–216.
- (28) Law, M.; Sirbuly, D. J.; Johnson, J. C.; Goldberger, J.; Saykally, R. J.; Yang, P. D. *Science* **2004**, *305*, 1269–1273.
- (29) Chinthalapudi, K.; Taft, M. H.; Martin, R.; Heissler, S. M.; Preller, M.; Hartmann, F. K.; Brandstaetter, H.; Kendrick-Jones, J.; Tsivaliaris, G.; Gutzeit, H. O.; Fedorov, R.; Buss, F.; Knolker, H. J.; Coluccio, L. M.; Manstein, D. J. *J. Biol. Chem.* **2011**, *286*, 29700–29708.
- (30) Sundberg, M.; Bunk, R.; Albet-Torres, N.; Kvennafors, A.; Persson, F.; Montelius, L.; Nicholls, I. A.; Ghatnekar-Nilsson, S.; Omling, P.; Tagerud, S.; Mansson, A. *Langmuir* **2006**, *22*, 7286–7295.
- (31) Lard, M.; Siethoff, L. T.; Mansson, A.; Linke, H. *Sci. Rep.* **2013**, *3*, 1092.
- (32) Lard, M.; Ten Siethoff, L.; Kumar, S.; Persson, M.; Te Kronnie, G.; Linke, H.; Mansson, A. *Biosens. Bioelectron.* **2013**, *48*, 145–152.
- (33) Sundberg, M.; Rosengren, J. P.; Bunk, R.; Lindahl, J.; Nicholls, I. A.; Tagerud, S.; Omling, P.; Montelius, L.; Mansson, A. *Anal. Biochem.* **2003**, *323*, 127–138.
- (34) Sheehan, P. E.; Whitman, L. J. *Nano Lett.* **2005**, *5*, 803–807.
- (35) Persson, M.; Albet-Torres, N.; Sundberg, M.; Ionov, L.; Diez, S.; Höök, F.; Månnsson, A.; Balaz, M. *Langmuir* **2010**, *26*, 9927–9936.
- (36) Korten, S.; Albet-Torres, N.; Paderi, F.; Ten Siethoff, L.; Diez, S.; Korten, T.; Te Kronnie, G.; Mansson, A. *Lab Chip* **2013**, *13*, 866–876.
- (37) Uyeda, T. Q.; Kron, S. J.; Spudich, J. A. *J. Mol. Biol.* **1990**, *214*, 699–710.
- (38) Roos, W.; Ulmer, J.; Grater, S.; Surrey, T.; Spatz, J. P. *Nano Lett.* **2005**, *5*, 2630–2634.